Sinter-hardening with concurrent improved plasticity in iron alloys induced by spark plasma sintering

Chao Yang,[a] Tian Wei, Xuebing Dong, Yuhua Li, Shengguan Qu, and Xiaoqiang Li
School of Mechanical & Automotive Engineering, National Engineering Research Center of Near-net-shape Forming for Metallic Materials, South China University of Technology, Guangzhou 510640, People's Republic of China

(Received 31 October 2013; accepted 19 March 2014)

We report on the occurrence of sinter-hardening with concurrent improved plasticity in fine-grained $Fe_{79.3}Mo_{4.5}P_{8.1}C_{6.75}B_{1.35}$ bulk alloys fabricated by spark plasma sintering (SPS) of metallic glass composite powder. When the sintering temperature is higher than the austenite transformation temperature, the as-fabricated bulk alloys are composed of expected wattle martensite plus Fe_3P, Fe_7C_3, and Fe_3Mo_3C. Meanwhile, the martensite-containing bulk alloys exhibit increased hardness, fracture strength as well as concurrent improved plasticity. The fracture stress and strain of the martensite-containing bulk alloys are as high as 2573 MPa and 8.6%, respectively. The formation of the martensite microstructure is attributed to that high sintering temperature leads to the austenitization transformation and consequently formed austenite partially transforms into martensite under rapid cooling rate provided by SPS system. The results obtained provide insight into fabrication of iron alloys with good mechanical property by powder metallurgy.

I. INTRODUCTION

Iron and its alloys are characterized by low cost, excellent mechanical properties, and large-scale production, and have been the most widely used structural materials. However, there is still a great demand for improving their mechanical properties. Using an appropriate method to fabricate bulk iron alloys with new structure and good combined mechanical properties has become an important research subject. As we all know, grain refinement is one of the most methods to improve mechanical properties. According to Hall–Patch relation, the strength of materials can be increased gradually by decreasing coarse grain to fine grain, ultrafine grain, and nanograin range.[1,2] Also, fabrication of different microstructure morphologies and distributions, such as bimodal-grained or multimodal-grained structure[3–5] and composite structure,[6–9] is an effective route to improve mechanical properties. In addition, improving mechanical properties can be achieved by obtaining some special phases. As a cost-effective route producing sintered parts, sinter-hardening can significantly improve mechanical properties by obtaining martensite microstructure resulted from rapid cooling from sintering temperature without the use of a traditional austenitization, oil quench, and tempering cycle.[10] In sinter-hardening, mechanical properties, or martensite content in iron alloys is mainly controlled by hardenability (carbon and alloy contents) and cooling rate.[11] Meanwhile, increased martensite content induces generally improved hardness, yield, and fracture strength but decreased plasticity.[12,13] Therefore, whether martensite microstructure can achieve sinter-hardening with concurrent improved plasticity in iron alloys becomes a significant academic question.

As an advanced material forming technology, the spark plasma sintering (SPS) method is widely used in fabricating metallic materials with new structures and improved properties[3–5,7,8,14–16] because of its relative low sintering temperature, short sintering time, and high heating rate. Especially, an outstanding advantage is that SPS can provide high heating and cooling rate while realizing a combination of sintering and subsequent thermal treatment.[17] Therefore, it becomes an interesting question whether martensite-containing iron alloys with sinter-hardening with concurrent improved plasticity in iron alloys can be fabricated by powder metallurgy.

In the present work, fine grained $Fe_{79.3}Mo_{4.5}P_{8.1}C_{6.75}B_{1.35}$ alloys with martensite microstructure were fabricated by SPS and crystallization of metallic glass composite powders. As expected, sinter-hardening with concurrent improved plasticity is induced in the martensite-containing bulk alloys. The results obtained can provide insight into fabrication of new structure in metallic materials with excellent properties by phase transformation design.

II. EXPERIMENTAL PROCEDURE

High purity (as-received powders had a purity of 99.9 wt.%) elemental powders of Fe, Mo, C, and B and industrial Fe–P intermediate compound powder consisting of 77.3 wt.% Fe and 21 wt.% P were used.

[a]Address all correspondence to this author.
e-mail: cyang@scut.edu.cn
DOI: 10.1557/jmr.2014.77

 © Materials Research Society 2014

https://doi.org/10.1557/jmr.2014.77 Published online by Cambridge University Press

Metallic glass composite powder with a stoichiometry of $Fe_{79.3}Mo_{4.5}P_{8.1}C_{6.75}B_{1.35}$ (atomic percentage) was synthesized by mechanical alloying after a milling time of 70 h. Detailed experimental process can be seen in elsewhere.[18] Subsequently, the synthesized metallic glass composite powder was precompacted, sintered, and crystallized in graphite die under a vacuum degree of 10^{-3} Pa at a pressure of 50 MPa by a SPS-825 system (Sumitomo Coal Mining Co. Ltd., Japan). To avoid the effect of carbon diffusion on martensitic transformation, inner walls of graphite die were put by a piece of thin tantalum paper. The sintered and crystallized bulk alloys were fabricated by heating to different sintering temperatures at a given heating rate and holding time or by heating to given sintering temperature at different heating rates. The as-fabricated samples have a cylindrical shape with a dimension of $\phi 10 \times 12$ mm. In addition, values of temperature (T) and time (t) during sintering and cooling process were recorded every 0.5 s by the attached software. The cooling rate of the as-fabricated samples was determined by calculating the slope of the time–temperature curve of the as-fabricated samples during the cooling process.

The phase constituent of the as-fabricated samples was characterized by x-ray diffraction (XRD) (D/max-2500/pc; Rigaku Corp., Tokyo, Japan) with Cu K_α radiation. The mechanical property of the as-fabricated samples was studied by uniaxial compression using a MTS TestStar 810 testing system at a strain rate of 5×10^{-4} s^{-1}. The size of the tested samples is designed as $\Phi 3 \times 6$ mm according to the ASTM E9-09 standards.[19] Vickers microhardness of the as-fabricated samples, obtained by calculating average value of ten measurement data, was investigated by using a Digital Microhardness Tester HVS-1000 (Shanghai Material Testing Machine Factory, China) and a load of 2.94 N applied for 20 s. The microstructure and fractography of the as-fabricated samples were observed by scanning electron microscope (SEM; Quanta 2000, FEI, Helsinki, Finland). In addition, transmission electron microscope (TEM, JEOL 3010, JEOL Ltd., Tokyo, Japan) was utilized for microstructure examination. The XRD patterns were fitted by the attached Jade5 software to determine the volume fraction (V) of α-Fe phase. The precise lattice parameter (a_0), with an uncertainty of $\pm 10^{-5}$ nm, of α-Fe phase in the as-fabricated samples was determined by suitable extrapolation of the variation of lattice parameter as a function of the Nelson-Riley parameter ($\cos^2\theta/\sin\theta + \cos^2\theta/\theta$).[20]

III. RESULTS AND DISCUSSION

To achieve high-density bulk alloys without melting phenomenon, the sintering temperature was chosen between 1073 and 1223 K. Figure 1 shows XRD patterns of the sintered and crystallized bulk alloys fabricated by heating to different sintering temperatures at 111 K/min and holding for 5 min. Before sintering, the synthesized metallic glass composite powder has a broad diffuse diffraction maximum located at $2\theta = 44.62°$, indicating perfect amorphous structure and sharp diffraction peaks indicating residual nanocrystalline α-Fe [Fig. 1(a)]. After sintering at temperature ranging from 1073 to 1223 K, the sintered and crystallized bulk alloys consist of four phases [Figs. 1(b)–1(d)], α-Fe(Mo), Fe_3P, Fe_7C_3, and Fe_3Mo_3C, respectively. When the sintering temperature reaches 1223 K, however, the diffraction peak intensity from α-Fe decreases dramatically [Fig. 1(e)]. This decrease may be attributed to the fact that the transformation of α-Fe into γ-Fe (called austenitization) occurs at enough high sintering temperature and subsequently formed austenite partially transforms into martensite under rapid cooling condition provided by SPS system. Due to overlap of diffraction peak position of martensite and α-Fe(Mo), it is difficult to distinguish them only by XRD patterns. Therefore, the sintered and crystallized bulk alloy fabricated at 1223 K may be composed of martensite with a relative big volume fraction, Fe_3P, Fe_7C_3, and Fe_3Mo_3C [Fig. 1(e)]. As listed in Table I, with the increased sintering temperature, the volume fraction of α-Fe(Mo) is 61.1%, 58.3%, 56.1%, and 50.6%, respectively. The decrease in the volume fraction of main α-Fe(Mo) phase demonstrates the increase in gross volume fraction of other phases. Meanwhile, the lattice parameter of α-Fe phase is larger than that of the standard value of α-Fe (Fig. 1 and Table I). This results from lattice expansion of Fe atoms dissolved by Mo atoms.

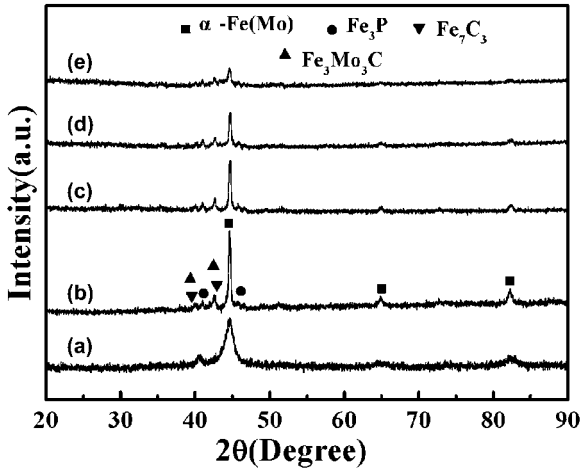


FIG. 1. (a) XRD pattern of the synthesized metallic glass composite powder after 70 h milling. XRD patterns of the sintered and crystallized bulk alloys fabricated by heating to different sintering temperatures at 111 K/min and holding for 5 min: (b) 1073 K, (c) 1123 K, (d) 1173 K, and (e) 1223 K, respectively.

Figure 2 shows XRD patterns of the sintered and crystallized bulk alloys fabricated by heating to 1203 K at 58 K/min and holding for different times. For better comparison to confirm phase transformation process,

https://doi.org/10.1557/jmr.2014.77 Published online by Cambridge University Press

TABLE I. Summary of the compression properties, volume fraction of α-Fe phase, relative density, and fitting XRD patterns for the sintered and crystallized bulk alloys. Young's modulus E, yield stress σ_y, strain at the yield point ε_y, ultimate compression stress σ_{max}, fracture strain ε_f, lattice parameter of the bcc α-Fe phase a_0, relative density ρ_{rt}, and microhardness H. The symbols x, y, and z in the sample S_{x-y-z} denote sintering temperature, heating rate, and holding time, respectively.

Samples	E (GPa)	σ_y (MPa)	ε_y (%)	σ_{max} (MPa)	ε_f (%)	V (vol%)	a_0 (Å)	ρ_{rt} (%)	H (GPa)
$S_{1073\text{-}111\text{-}5}$	37.6	...	3.2	1198	3.2	61.1	2.8759	90.2	5.98
$S_{1123\text{-}111\text{-}5}$	44.1	...	3.6	1617	3.6	58.3	2.8725	98.0	6.26
$S_{1173\text{-}111\text{-}5}$	39.7	...	4.8	1856	4.8	56.1	2.8765	98.3	6.34
$S_{1223\text{-}111\text{-}5}$	42.3	2163	5.3	2573	8.6	50.6	...	98.9	6.75
$S_{1203\text{-}58\text{-}0}$	43.6	1412	3.4	1722	4.5	66.5	2.8760	98.6	6.39
$S_{1203\text{-}58\text{-}5}$	43.7	1848	4.4	2238	5.9	56.3	2.8783	98.7	6.56
$S_{1203\text{-}58\text{-}10}$	43.2	1923	4.7	2179	6.2	48.7	2.8798	98.8	6.66
$S_{1203\text{-}58\text{-}15}$	41.1	2032	4.9	2292	7.0	53.2	2.8790	98.8	6.67
$S_{1203\text{-}58\text{-}20}$	43.4	1875	4.8	2192	7.7	50.1	2.8782	98.8	6.65

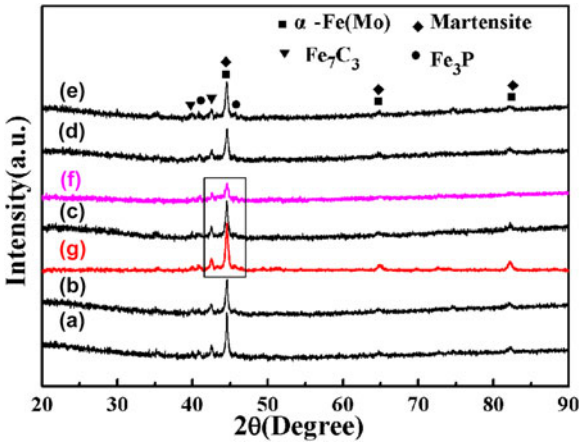


FIG. 2. XRD patterns of the sintered and crystallized bulk alloys fabricated by heating to 1203 K at 58 K/min and holding for different times: (a) 0 min, (b) 5 min, (c) 10 min, (d) 15 min, and (e) 20 min, respectively. (f) represents XRD pattern of the sintered and crystallized bulk alloys fabricated by heating to 1223 K at 111 K/min and holding for 5 min, namely the XRD pattern of the sintered sample $S_{1223\text{-}111\text{-}5}$; (g) represents XRD pattern of the sintered and crystallized bulk alloy fabricated by heating to 1123 K at 52 K/min and holding for 10 min, namely the XRD pattern of the sintered sample $S_{1123\text{-}52\text{-}10}$.

XRD patterns of the samples $S_{1223\text{-}111\text{-}5}$ [Fig. 2(f)] and $S_{1123\text{-}52\text{-}10}$ [Fig. 2(g)] are added. Obviously, three XRD patterns corresponding to the sintering temperatures of 1123, 1203, and 1223 K in the black frame indicate that with the increased sintering temperature the intensity of α-Fe diffraction peak decreases gradually. Especially, at a sintering temperature of 1223 K, the intensity of α-Fe diffraction peak degrades significantly due to formation of martensite with a relative big volume fraction. Based on this phase transformation process, a medium temperature of 1203 K is chosen to emphatically investigate the effect of holding time on the transformation process of martensite. Apparently, all samples contain mixed α-Fe and martensite phases, Fe_3P, and Fe_7C_3. With the extended holding time, the intensity of α-Fe diffraction peaks decreases gradually [Figs. 2(a)–2(d)]. However, with further extended holding time to 20 min, the intensity of α-Fe diffraction peaks increases instead [Fig. 2(e)]. In the whole process, the change in the intensity of α-Fe diffraction peaks embodies the variation in the volume fraction of the formed martensite phase. As listed in Table I, with the extended holding time, the volume fractions of α-Fe(Mo) are 66.5%, 56.3%, 53.2%, 48.7%, and 50.1% [Figs. 2(a)–2(e)], respectively.

Figure 3 presents SEM micrographs of the sintered and crystallized bulk alloys fabricated by heating to different sintering temperatures at 111 K/min and holding for 5 min. The sample $S_{1073\text{-}111\text{-}5}$ with a low relative density of 90.2% has distinct holes located around the boundaries of powder particles. Meanwhile, the precipitation of the Fe_3P from α-Fe matrix is inadequate and asymmetric. With the increased sintering temperature to 1123 K, the relative density of the sample $S_{1123\text{-}111\text{-}5}$ increases to 98.0% and the precipitation of the Fe_3P is more uniform [Fig. 3(a)]. With further increased sintering temperature to 1173 K, the back scattering micrograph of the sample $S_{1173\text{-}111\text{-}5}$ shows that except for the precipitation of Fe_3P and α-Fe matrix, Fe_3Mo_3C and Fe_7C_3 phases exist according to the results of XRD pattern and energy spectrum analysis [Fig. 2(d)]. However, when the sintering temperature increases to 1223 K, the microstructure of the sample $S_{1223\text{-}111\text{-}5}$ is different from those of other samples [Fig. 2(c)]. It can be seen that many parallel wattles similar to wattle martensite form accordingly. Moreover, TEM micrograph of the sample $S_{1223\text{-}111\text{-}5}$ displays formed martensite phases and various gray dislocations in the white region (Fig. 4), further confirming the presence of wattle martensite. Besides, energy diffraction spectrum and spot analysis prove that ultrafine particle with a grain size of 300–400 nm is Fe_3Mo_3C and the gray banding phase is Fe_3P, in accordance with the results of SEM microstructure in Fig. 3(c). The grain size of the Fe_7C_3 and wattle martensite is about 3–6 μm and 3–5 μm, respectively. In addition, the microstructure suggests that the volume fraction of the α-Fe phase decreases with the increased sintering temperature, in accordance with the results of the XRD patterns in Fig. 1.

https://doi.org/10.1557/jmr.2014.77 Published online by Cambridge University Press

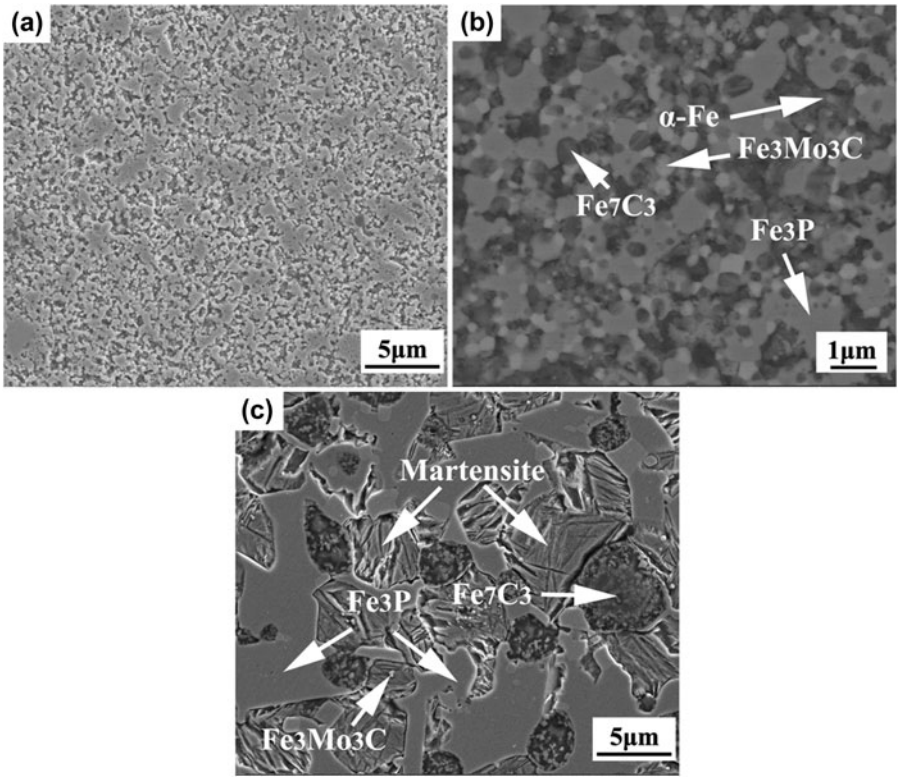


FIG. 3. SEM micrographs of the sintered and crystallized bulk alloys fabricated by heating to 1123 K (a), 1173 K (b) (back scattering micrograph), and 1223 K (c) at 111 K/min and holding for 5 min.

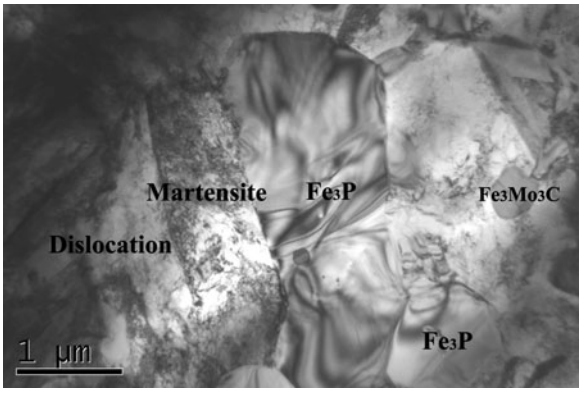


FIG. 4. TEM micrograph of the sintered and crystallized bulk alloy fabricated by heating to 1223 K at 111 K/min and holding for 5 min.

Figure 5 presents SEM micrographs of the sintered and crystallized bulk alloys fabricated by heating to 1203 K at 58 K/min and holding for different times. Obviously, all samples consist of the mixed phases of α-Fe and martensite, Fe_3P, and Fe_7C_3, in accordance with the results of XRD pattern in Fig. 2. Under no holding condition, there is no enough time for austenite to nucleate and grow and thus the obtained martensite has a relative low volume fraction [Fig. 5(a)]. Its microstructure encompasses precipitated Fe_3P phase distributed on the matrix of α-Fe and martensite and Fe_7C_3 particles dispersed therein. With the prolonged holding time, the volume fraction of martensite gradually increases in contrast to the decreased volume fraction of α-Fe. After holding for 15 min [Fig. 5(b)], the volume fraction of martensite achieves a maximum value. With further prolonged holding time to 20 min [Fig. 5(c)], the volume fraction of martensite decreases slightly accompanied with the finer wattle martensite. Therefore, holding time has apparent effect on formation and growth of martensite and further affects mechanical properties of the sintered and crystallized bulk alloys.

Figure 6 presents room-temperature compression engineering stress–strain curves of the sintered and crystallized bulk alloys fabricated by heating to different sintering temperatures at 111 K/min and holding for 5 min. The corresponding mechanical properties are listed in Table I. With the increased sintering temperature, the fracture stress and strain are 1198 MPa and 3.2% ($S_{1073\text{-}111\text{-}5}$), 1617 MPa and 3.6% ($S_{1123\text{-}111\text{-}5}$), 1856 MPa and 4.8% ($S_{1173\text{-}111\text{-}5}$), and 2573 MPa and 8.6% ($S_{1223\text{-}111\text{-}5}$), respectively. Obviously, the samples exhibit no plasticity and relative low fracture stress when the sintering temperatures are lower than 1223 K. However, the sample fabricated at the sintering temperature of 1223 K has distinct plasticity and high compressive yield and fracture stresses. Meanwhile, with the increased sintering temperature, the microhardness increases from 5.98 GPa ($S_{1073\text{-}111\text{-}5}$),

https://doi.org/10.1557/jmr.2014.77 Published online by Cambridge University Press

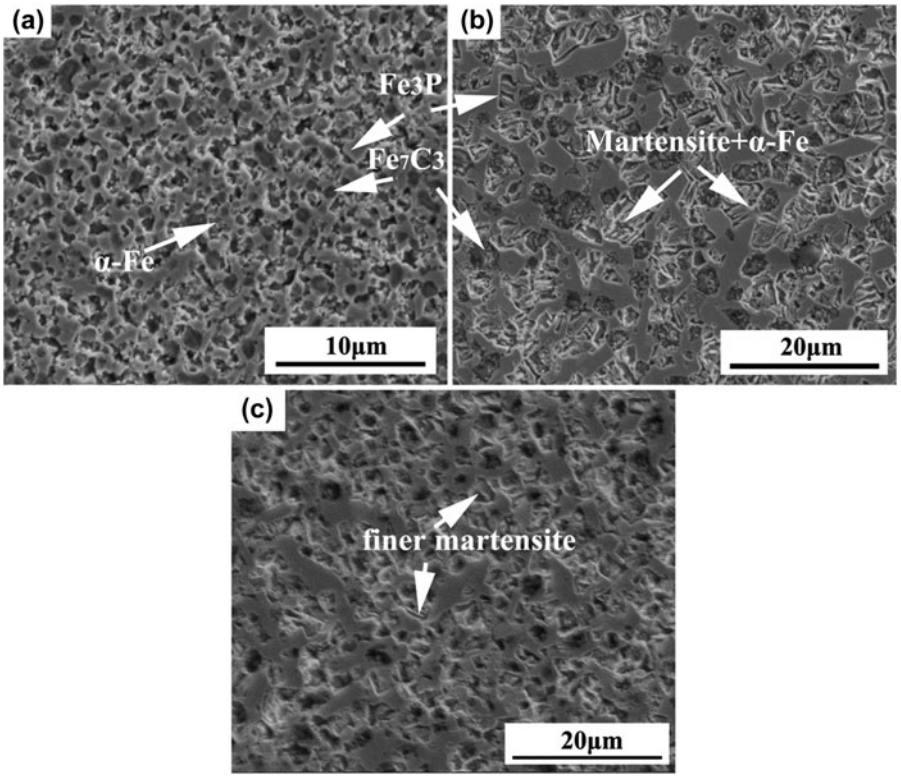


FIG. 5. SEM micrographs of the sintered and crystallized bulk alloys fabricated by heating to 1203 K at 58 K/min and holding for different times: (a) 0 min, (b) 15 min, and (c) 20 min, respectively.

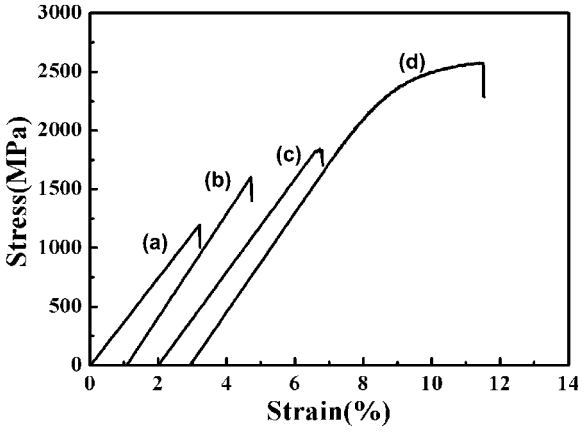


FIG. 6. Room-temperature compression engineering stress–strain curves of the sintered and crystallized bulk alloys fabricated by heating to different sintering temperatures at 111 K/min and holding for 5 min: (a) 1073 K, (b) 1123 K, (c) 1173 K, and (d) 1223 K, respectively.

6.26 GPa ($S_{1123\text{-}111\text{-}5}$), 6.34 GPa ($S_{1173\text{-}111\text{-}5}$) to 6.75 GPa ($S_{1223\text{-}111\text{-}5}$), respectively. This indicates the occurrence of sinter-hardening with concurrent improved plasticity in the sample $S_{1223\text{-}111\text{-}5}$ in our case. This is quite interesting and it is believed to be relevant to the microstructures of the sintered and crystallized bulk alloys shown in Figs. 3 and 4. When the sintering temperatures are lower than 1223 K, the samples include four phases, i.e., α-Fe, Fe_3P, Fe_7C_3, and Fe_3Mo_3C. The multiphase structure usually makes deformation very complicated compared with two-phase structure.[14–16,21] It is quite difficult to produce the effect that one phase hinders propagation of dislocation and shear band generated in the other phase and thus the bulk sample exhibits distinct plasticity. Therefore, the samples $S_{1073\text{-}111\text{-}5}$, $S_{1123\text{-}111\text{-}5}$, and $S_{1173\text{-}111\text{-}5}$ (Fig. 6 and Table I) have no plasticity. However, it is worthwhile noting that the sample $S_{1223\text{-}111\text{-}5}$ [Fig. 6(d)] has significantly sinter-hardening with concurrent improved plasticity. This may be attributed to the formation of wattle martensite phase [Fig. 3(c)]. As shown in Fig. 4, wattle martensite has a lot of high-density dislocations with an asymmetrical distribution. The low-density dislocation regions provide the place of movement for dislocation. And the movement of dislocation can relieve the effect of stress concentration and thus favor the improvement of plasticity of bulk materials.[22] Furthermore, the quenching stress generated during sintering and cooling is small and no microflaw forms and thus it is difficult for microflaw to spread through martensite strips. Besides, coarse Fe_7C_3 particles have active influence on restraining the spread of microflaw. These aspects are contributed to the increase in fracture stress and the improvement in plasticity for the martensite-containing bulk samples. As for the sintered and crystallized bulk alloys fabricated by heating to 1203 K at 58 K/min and holding for different times, their mechanical

https://doi.org/10.1557/jmr.2014.77 Published online by Cambridge University Press

properties are closely related to microstructure changes. Except that the sample $S_{1203\text{-}58\text{-}0}$ has low fracture strength and strain, other samples exhibit obvious plasticity (Table I). It can be seen that similar to the variation in the volume fraction of formed lath martensite, the fracture strength and strain of the samples increase first and then decreases with the prolonged holding time (Fig. 5 and Table I). This proves that formed lath martensite indeed exerts significant effect on mechanical properties of the sintered and crystallized bulk alloys. When the holding time is below 15 min, the increased volume fraction of formed lath martensite leads to the increase in strength and ductility (Fig. 5 and Table I). However, when the holding time reaches 20 min, carbide coarsening is serious and the size of lath martensite is large. This may be the reason for the sudden decrease in the strength and the increase in the plasticity for the sample $S_{1203\text{-}58\text{-}20}$.

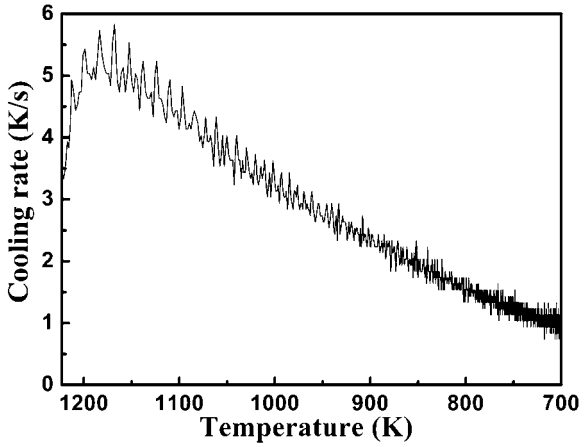


FIG. 7. Variation of the cooling rate as a function of the temperature for the sintered and crystallized bulk alloys fabricated by heating to 1223 at 111 K/min and holding for 5 min.

As discussed above, sinter-hardening with concurrent improved plasticity reported here is closely related to the formation of martensite microstructure. The formation of lath martensite in our case is attributed to three factors, i.e., austenitization, carbon content, and cooling rate. In sintering process, high sintering temperature at 1223 K leads to the transformation of α-Fe into γ-Fe (called austenitization) and consequently formed austenite partially transforms into martensite under rapid cooling condition provided by SPS system. Secondly, although Fe_7C_3 and Fe_3Mo_3C formed in the sintered and crystallized bulk alloys deplete a portion of carbon atoms, high carbon content of 1.55 wt.% C in present alloy system guarantees enough carbon atoms dissolved into α-Fe and thus promotes the formation of lath martensite under rapid cooling condition. Most important of all, high cooling rate provided by SPS system is a decisive factor for the formation of lath martensite. It is well accepted that depending on the

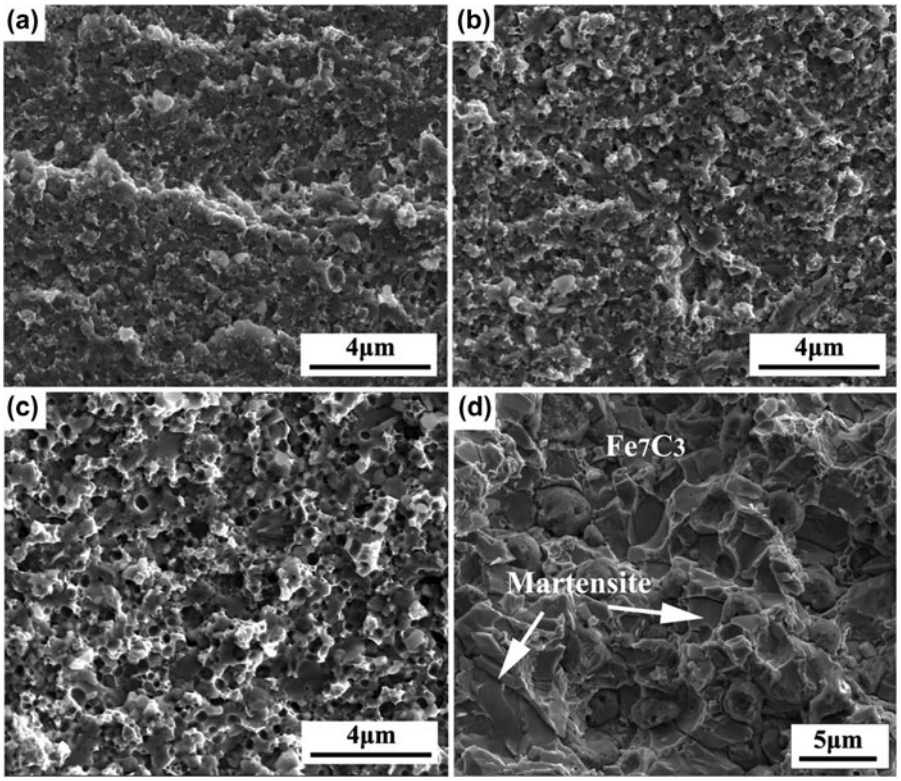


FIG. 8. SEM fracture micrographs of the sintered and crystallized bulk alloys fabricated by heating to different sintering temperatures at 111 K/min and holding for 5 min: (a) 1073 K, (b) 1123 K, (c) 1173 K, and (d) 1223 K, respectively.

https://doi.org/10.1557/jmr.2014.77 Published online by Cambridge University Press

composition and the mass of the component, commonly, the cooling rates of 0.5–1 K/s within the temperature range of 900–425 °C are required to form martensitic microstructure in sinter-hardening.[11,12,23] As shown in Fig. 7, the cooling rates within the temperature range of 900–425 °C are higher than that 0.5–1 K/s for the sintered and crystallized bulk alloys. Therefore, high cooling rate provided by SPS system further promotes the formation of martensite microstructure.

Figure 8 exhibits SEM fracture micrographs of the sintered and crystallized bulk alloys fabricated by heating to different sintering temperatures at 111 K/min and holding for 5 min. When the sintering temperature is lower than 1223 K, the fractured surfaces of the samples present apparently brittle mode with river pattern and tongue pattern [Figs. 8(a)–8(c)]. In contrast, when the sintering temperature reaches 1223 K, the sample $S_{1223\text{-}111\text{-}5}$ displays the fracture features of honeycomb and intergranular fracture [Fig. 8(d)]. Besides, it is proved again that the grain size of the samples increases with the increased sintering temperature. Especially, the grain size of the sample $S_{1223\text{-}111\text{-}5}$ is between 3 and 5 μm, achieving fine grained regime in contrast to ultrafine-grained structure obtained at relative low sintering temperatures.

IV. CONCLUSION

Fine grained $Fe_{79.3}Mo_{4.5}P_{8.1}C_{6.75}B_{1.35}$ bulk alloys with high strength and distinct plasticity were fabricated by SPS and crystallization of amorphous phase. Results show that sinter-hardening with concurrent improved plasticity is induced in the as-fabricated bulk alloys. When the sintering temperature is lower than the austenite transformation temperature, the as-fabricated bulk alloys consist of four phases, α-Fe(Mo), Fe_3P, Fe_7C_3, and Fe_3Mo_3C and exhibit no plasticity with low fracture stress. In contrast, when the sintering temperature is above the austenite transformation temperature, the as-fabricated bulk alloys are composed of four phases, i.e., wattle martensite, Fe_3P, Fe_7C_3, and Fe_3Mo_3C and display obvious plasticity with high fracture stress. The good combination between strength and plasticity results from the formation of wattle martensite. The results obtained provide insight into fabrication of iron alloys with good mechanical property by powder metallurgy.

ACKNOWLEDGMENTS

This work was supported by the Guangdong Natural Science Foundation (No. S2013010012147), the Science and Technology Innovation Project of Higher School of Guangdong Province (No. 2012KJCX0010), the Fundamental Research Funds for the Central Universities (No. 2013ZZ0008), the Program for New Century Excellent Talents in University (No. NCET-11-0163), and the Excellent Young Talents of South China University of Technology.

REFERENCES

1. Q. Wei, L. Kecskes, T. Jiao, K.T. Hartwig, K.T. Ramesh, and E. Ma: Adiabatic shear banding in ultrafine-grained Fe processed by severe plastic deformation. *Acta Mater.* **52**(7), 1859–1869 (2004).
2. B.Q. Han, F.A. Mohamed, and E.J. Lavernia: Mechanical properties of iron processed by severe plastic deformation. *Metall. Mater. Trans. A* **34**(1), 71–83 (2003).
3. B. Srinivasarao, K. Oh-ishi, T. Ohkubo, T. Mukali, and K. Hono: Synthesis of high-strength bimodally grained iron by mechanical alloying and spark plasma sintering. *Scripta Mater.* **58**(9), 759–762 (2008).
4. H.W. Zhang, R. Gopalan, T. Mukai, and K. Hono: Fabrication of bulk nanocrystalline Fe–C alloy by spark plasma sintering of mechanically milled powder. *Scripta Mater.* **53**(7), 863–868 (2005).
5. C. Yang, T. Wei, Y.P. Yao, Y.H. Li, S.G. Qu, and L.C. Zhang: Bulk multimodal-grained irons with large plasticity fabricated by spark plasma sintering. *Mater. Sci. Eng., A* **591**, 54–58 (2014).
6. S.F. Guo, L. Liu, N. Li, and Y. Li: Fe-based bulk metallic glass matrix composite with large plasticity. *Scripta Mater.* **62**(6), 329–332 (2010).
7. Y.Y. Li, C. Yang, W.P. Chen, X.Q. Li, and S.G. Qu: Ultrafine-grained $Ti_{66}Nb_{13}Cu_8Ni_{6.8}Al_{6.2}$ composites fabricated by spark plasma sintering and crystallization of amorphous phase. *J. Mater. Res.* **24**(6), 2118–2122 (2009).
8. Y.Y. Li, C. Yang, S.G. Qu, X.Q. Li, and W.P. Chen: Nucleation and growth mechanism of crystalline phase for fabrication of ultrafine-grained $Ti_{66}Nb_{13}Cu_8Ni_{6.8}Al_{6.2}$ composites by spark plasma sintering and crystallization of amorphous phase. *Mater. Sci. Eng., A* **528**(1), 486–493 (2010).
9. D. Vallauri, A. Atías, and A. Chrysanthou: TiC-TiB_2 composites: A review of phase relationships, processing and properties. *J. Euro. Ceram. Soc.* **28**, 1697–1713 (2008).
10. W.B. James: *What is Sinter-Hardening. Advances in Powder Metallurgy and Particulate Materials* (Metal Powder Industries Federation, Princeton, NJ, 1998).
11. J.M. Capus: Sinter-hardening offers high strength at lower cost. *Metal Powder Report* **52**(9), 17–18 (1997).
12. M.L. Marucci, G. Fillari, P. King, and K.S.S. Narasimhan: Sintering a path to cost-effective hardened parts. *Metal Powder Report* **60**, 42–46 (2005).
13. Z.Y. Xiao, M.Y. Ke, L. Fang, M. Shao, and Y.Y. Li: Die wall lubricated warm compacting and sintering behaviors of pre-mixed Fe-Ni-Cu-Mo-C powders. *J. Mater. Process. Tech.* **209**, 4527–4530 (2009).
14. Y.Y. Li, C. Yang, T. Wei, X.Q. Li, and S.G. Qu: Ductile fine-grained Ti-O-based composites with ultrahigh compressive specific strength fabricated by spark plasma sintering. *Mater. Sci. Eng., A* **528**, 1897–1900 (2011).
15. C. Yang, L.H. Liu, Q.R. Cheng, D.D. You, and Y.Y. Li: Equiaxed grained structure: A structure in titanium alloys with higher compressive mechanical properties. *Mater. Sci. Eng., A* **580**, 397–405 (2013).
16. Y.Y. Li, L.M. Zou, C. Yang, Y.H. Li, and L.J. Li: Ultrafine-grained Ti-based composites with high strength and low modulus fabricated by spark plasma sintering. *Mater. Sci. Eng., A*, **560**, 857–861 (2013).
17. Z. Munir, U.A. Tamburini, and M. Ohyanagi: The effect of electric field and pressure on the synthesis and consolidation of materials: A review of the spark plasma sintering method. *J. Mater. Sci.* **41**, 763–777 (2006).
18. C. Yang, T. Wei, J. Zeng, L.H. Liu, S.G. Qu, and Y.Y. Li: Microstructure evolution and thermal properties in FeMoPCB alloy during mechanical alloying. *J. Non-Cryst. Solids* **358**, 1459–1464 (2012).
19. Standard Test Methods of Compression Testing of Metallic Materials at Room Temperature. (ASTM, 2009). http://www.astm.org/Standards/E9.htm

https://doi.org/10.1557/jmr.2014.77 Published online by Cambridge University Press

20. B.D. Cullity: *Elements of X-ray Diffraction* (Addison-Wesley, Reading, MA, 1978); pp. 102 and 356.
21. A. Sreeramamurthy, M. Harold, A.G. Charles, W.N. Brett, and P.G. Oberson: Mechanical properties of alloys consisting of two ductile phases. *Prog. Mater. Sci.* **51**, 632–709 (2006).
22. R.E. Smallman and A.H.W. Ngan: Plastic Deformation and Dislocation Behaviour. In *Modern Physical Metallurgy (8 th ed)*. (Elsevier, New York, NY, 2014); 357–414.
23. P.B. MPIF: *Powder Metallurgy Design Manual*, 3rd ed. Metal Powder Industries Federation: Princeton, NJ, 1998.

https://doi.org/10.1557/jmr.2014.77 Published online by Cambridge University Press